Phase Structures, Transition Behaviors, and Surface Alignment in Polymers Containing Rigid-Rodlike Backbones with Flexible Side Chains. 1. Monotropic Phase Behavior in a Main-Chain/Side-Chain Liquid Crystalline Polyester

Jason J. Ge, Anqiu Zhang, Kevin W. McCreight, Rong-Ming Ho, Shy-Yeu Wang, Xiaoming Jin, Frank W. Harris, and Stephen Z. D. Cheng*

Maurice Morton Institute and Department of Polymer Science, The University of Akron, Akron, Ohio 44325-3909

Received May 1, 1997; Revised Manuscript Received July 22, 1997[⊗]

ABSTRACT: A series of polyesters, which are comprised of aromatic main chain backbones and flexible aliphatic side chains with 4-cyanobiphenyl end groups, has been synthesized based on a polycondensation of 2,2′-bis(trifluoromethyl)-4,4′-biphenyldiyldicarbonyl chloride with 2,2′-bis{ω-[(4-(4-cyanophenyl)phenoxy]-*n*-alkoxy)carbonyl]}-4,4′-biphenyldiol (PEFBP). For a PEFBP polyester containing eleven methylene units in the side chains, PEFBP($n = 11$), multiple phase transitions can be found *via* differential scanning calorimetry during cooling and heating at varying rates. Different phase structures are identified by wide-angle X-ray diffraction and electron diffraction experiments, while morphologies of these ordered states are observed by polarized light and transmission electron microscopy. During cooling, a high temperature nematic (N) phase is formed at 193 °C independent of the cooling rate due to the combined orientational order of the cyanobiphenyl groups in the side chains and the aromatic polyester backbones. At a temperature of 90 °C, a new ordered low-temperature phase with an orthorhombic lattice (K_O) starts to form at a cooling rate equal to or slower than 10 °C/min. However, the formation temperature of this phase is too close to the glass transition temperature (60 °C) to proceed to completion. Only at very slow heating rates (e.g., 1 °C/min), can the K_O phase further develop. This phase melts at around 120 °C during heating and returns to the N phase. A new crystalline phase with a triclinic lattice at high temperatures (K_{T1}) appears at 130 °C. It then transfers to a second triclinic crystalline phase (K_{T2}). This K_{T2} phase melts at around 180 °C and, again, returns to the N phase. At 193 °C, isotropization occurs. This complicated phase behavior can be explained by the monotropic origin of the K_O and K_{T1} phases with respect to the K_{T2} phase, which are metastable in the whole temperature region.

Introduction

In recent years, a number of publications have focused on the synthesis and structural characterization of rigid-rodlike polymer backbones with flexible side chains.[1−12] The backbones can be aromatic polyesters, polyanhydrides, polyamides, poly(benzobisoxazoles), poly(azomethines) and poly(glutamates). For flexible side chains, most of the studies have concentrated on different lengths of alkyl side chains (different numbers of methylene units). The connections with a phenylene ring are usually ether, ester, or thio groups at mono, bis, or tetrakis positions on one backbone phenylene group. Since the rigid-rodlike backbone and flexible side chain are usually not miscible, these two components tend to be separated. Molecular packing is often considered to be two-dimensional single chains stacked with other chains to form a three-dimensional structure. The rigid-rodlike backbones aggregate to form a sheet-like structure along one direction of lateral packing between two side chain layers. Recently, a hexagonal packing has also been speculated based on powder wide-angle X-ray diffraction (WAXD).[13]

What influence the alkyl side chains have on the structural formation of the phases in these polymers is always one of the major questions in the condensed state characterization of these materials. Structures ranging from low-ordered liquid crystal to three-dimensional long-range-ordered crystal phases have been reported. Two extreme views of the backbone environments in the materials are that (1) the rigid-rodlike backbones are immersed in an alkyl liquid medium or (2) the backbone chains and alkyl side groups participate in the same crystalline lattice. Since almost every sample shows layer structures due to the separation of the side chains from the backbones, it is generally recognized that the existence of the liquid crystalline phases are due to the rigid-rodlike backbone chains. Most reports classify these phases as smectic-like, hexagonal-like or sanidic liquid crystalline phases. These phases may be formed by supramolecular packing with larger lattice sizes.

This class of polymers may potentially be important for technological applications such as alignment layers in liquid crystal displays (LCDs) to obtain high pretilt angles. After the polymer is coated onto the glass substrate, mechanical rubbing can be applied to the polymer thin layer surfaces. This procedure generates pretilt angles on the layer surface which are necessary to orient liquid crystal molecules along a specific direction in twisted or supertwisted nematic LCDs. Methylene side chains with cyanobiphenyl groups may help to achieve high orientational efficiency of the liquid crystalline molecules in LCDs. Along this research line, we have synthesized a series of aromatic polyesters with alkyl side chain groups based on the polycondensation of 2,2′-bis(trifluoromethyl)-4,4′-biphenyldiyldicarbonyl chloride with 2,2′-bis{ω-[(4-(4-cyanophenyl)phenyoxy]-*n*-alkoxy)carbonyl]}-4,4′-biphenyldiol.[14] The generalized chemical structure of this series of polymers is

* To whom correspondence should be addressed.
[⊗] Abstract published in *Advance ACS Abstracts,* September 15, 1997.

S0024-9297(97)00611-6 CCC: $14.00

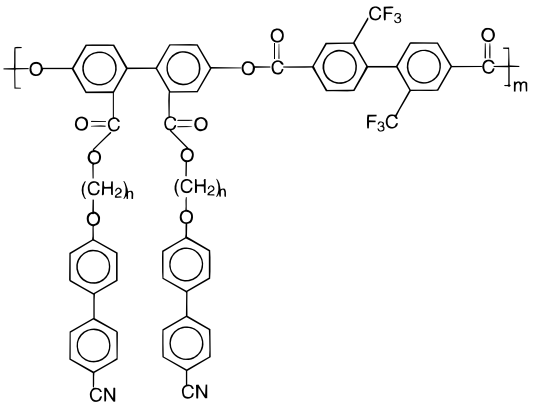

with $n = 6-12$, and is abbreviated as PEFBP(n). From these polymers, the polyester containing eleven methylene units in the side chains, PEFBP($n = 11$), will be addressed in this publication.

It is well-known that commercialized E7 liquid crystal molecules from Merck are a mixture of cyanobiphenyls with different lengths of methylene end groups. For a cyanobiphenyl with 11 methylene units, it is a crystal (K) phase that is found which melts at 71.5 °C to enter a smectic A (S_A) phase and this S_A phase reaches the isotropic melt at 87.5 °C.[15] When the cyanobiphenyl molecules are grafted onto flexible polymer backbones as side groups, such as polyacrylate($n = 11$), liquid crystalline behavior is still maintained in this side-chain liquid crystalline polymer. It has a S_A phase and reaches the isotropic melt at 145 °C with a heat of transition of 2.6 kJ/mol.[16] Note that the $S_A \leftrightarrow I$ transition temperature increases more than 55 °C when the small molecule is incorporated into the polymer. This phenomenon has also been reported in polyoxetane backbone chains with methylene side chains having cyanobiphenyl end groups.[17] It is interesting to compare the transition behavior when the cyanobiphenyl groups are connected with rigid-rodlike backbones *via* methylene units as in the present case. In this publication, it will be shown that this rigid-rodlike polyester having methylene units with cyanobiphenyl end groups exhibits a complicated phase transition behavior, which may result from the existence of monotropic phases.

Experimental Section

Materials and Samples. A series of polyesters containing rigid-rodlike backbones with methylene units and cyanobiphenyl groups was synthesized based on the procedure in ref 14. For PEFBP($n = 11$), its molecular weight per repeating unit is 1304 g/mol in which 520 belongs to the main chain and 784 is due to the side groups. The intrinsic viscosity of this polymer is 0.5 dL/g in chloroform. An estimated degree of polymerization is around 10−15. Thermal degradation experiments showed that in a dry nitrogen atmosphere, 2% weight loss of the sample was at 350 °C at a heating rate of 10 °C/min.

Polyester film samples (thickness of about 50 μm) were solution cast and vacuum-dried and were used in differential scanning calorimetry (DSC) and WAXD powder experiments. For WAXD structural determination, fiber samples were spun from the nematic state and were annealed at different temperatures below those of the specific transitions. Thin films were prepared from a solution casting method with film thicknesses of less than 0.3 μm for transmission electron microscopy (TEM) and electron diffraction (ED) experiments.

Equipment and Experiments. DSC was performed on a Perkin-Elmer DSC-7 with a cooling apparatus. The temperature and heat flow were calibrated using standard materials at different cooling rates between 1 and 40 °C/min. When the cooling and heating rates are high, the sample weights were reduced correspondingly in order to avoid thermal gradients within the samples. To determine the transition temperatures, onset temperatures were used. For cooling experiments, onset temperatures were obtained on the high-temperature side, while for heating experiments, those temperatures were from the low-temperature side. The heating and cooling cycles were also utilized in order to examine the reversibility of the thermal transitions and thermal stability of the samples.

Reflection WAXD experiments were conducted with a Rigaku 12 kW rotating-anode generator (Cu Kα) coupled with a Geigerflex D/max-RB diffractometer (with a radius of 185 mm). The X-ray beam was line focused and monochromatized using a graphite crystal. The beam size was controlled by the slit system (a divergence slit of 0.5°, a receiving slit of 0.15 mm, and a scattering slit of 0.5°). The reflection peak positions and widths were carefully calibrated with silicon crystals of known crystal size in a high angle region ($>2\theta = 15°$) and silver behenate in a low angle region ($<2\theta = 15°$). The angular deviation measured in WAXD was ±0.05° with an instrumentation function of 0.03°. For WAXD powder patterns taken at room temperature, a scanning rate of 0.5°/min was used in the 2θ angle region of 1.5−35°. The heating and cooling experiments at 1 °C/min were also performed on WAXD with a hot stage. The scanning rate in this case was 7.0°/min in the selected 2θ angle range. Background scattering was carefully recorded and subtracted from the WAXD patterns. In order to accurately determine the d-spacings of the reflections, isothermal WAXD experiments were conducted at the fiber annealing temperatures after the samples were annealed for a prolonged time. Fiber WAXD patterns were obtained using a flat-plate vacuum camera attached to a Rigaku tube X-ray generator. Exposure times were allowed to range from 1 to 5 days in order to identify both strong and weak reflections. The same calibration procedure described previously was followed. The unit cell determination procedure based on reciprocal lattice approach was described in detailed in one of our early publications.[18] Computer refinement was conducted to achieve the fit with the least error between experimental results and calculated data based on a continuous refinement program established in our laboratory.[18]

PLM observations were performed on an Olympus (HB-2) microscope coupled with a Mettler (FP82) hot stage, while a JEOL (1200 EX II) TEM was utilized to study morphology and to determine ordered structures in the sample. An accelerating voltage of 120 kV was used in the TEM. The thin polyester films were shadowed by Pt and coated with carbon for TEM observations. For ED experiments, a tilting stage was also used to determine all three dimensions of the unit cells. Calibration of the ED spacing was done using TlCl in a d-spacings range smaller than 0.384 nm, which is the largest spacing for TlCl. Spacing values larger than 0.384 nm were calibrated by doubling the d-spacing of those reflections based on their first-order reflections. The thermal histories of the polyester films were the same as those in WAXD experiments.

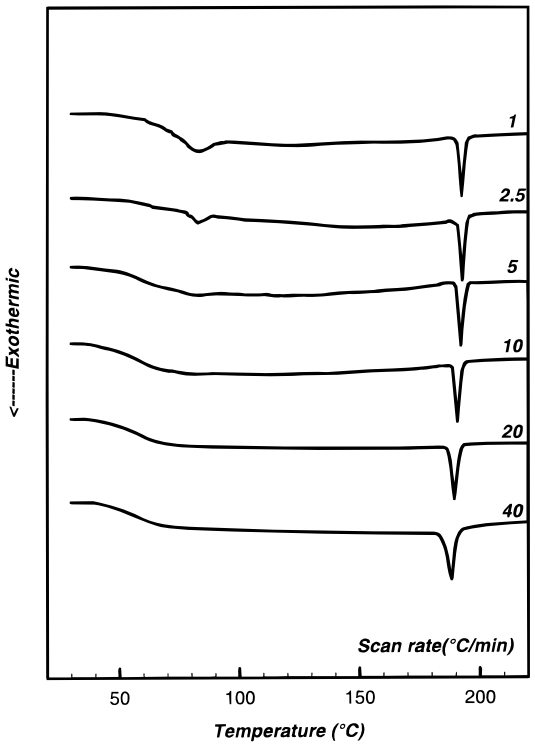

Figure 1. Set of PEBFP(n = 11) DSC cooling curves from the isotropic melt to room temperature at different cooling rates.

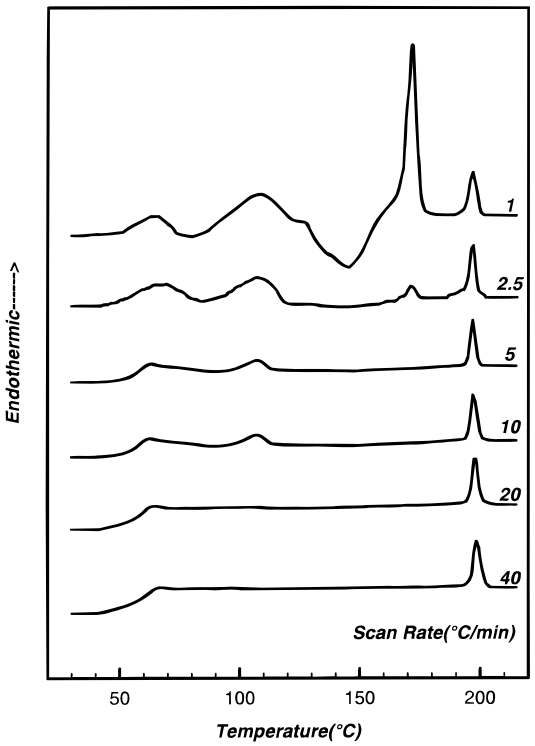

Figure 2. Set of PEBFP(n = 11) DSC heating curves from room temperature to the isotropic melt at different heating rates.

Results and Discussion

Phase Transition Behavior. Figures 1 and 2 show two sets of DSC cooling and subsequent heating diagrams at different rates (between 1 and 40 °C/min) for PEFBP(n = 11). Over the whole cooling rate range studied (Figure 1), one high-temperature exothermic onset can be found at around 193 °C. This transition temperature onset and the heat of transition (2.4 kJ/mol) of this exothermic peak are cooling rate independent. When the cooling rate is 10 °C/min or slower, a low-temperature exothermic peak can also be observed with an onset temperature around 90 °C. Again, this transition temperature shows little cooling rate dependence. However, the heat of transition increases with decreasing cooling rate. Note that this transition is close to the glass transition temperature of this polymer (60 °C). It is speculated that at least the high-temperature exothermic process found during cooling may be associated with a liquid crystalline transition, which generally does not exhibit cooling rate dependence.

During heating above a rate of 10 °C/min, as shown in Figure 2, it seems that only the high-temperature endothermic onset can be found at 193 °C. However, at heating rates of 10 °C/min or slower, a low-temperature endothermic peak starts to appear at an onset temperature of 100 °C (a peak temperature of 108 °C). The heat of transition increases with decreasing heating rate since slow heating may provide additional opportunities to develop this ordered structure. At the slow heating rate, a small exothermic process can also be seen just above the glass transition temperature (around 80 °C) and below the endothermic peak at 100 °C. This may be associated with the further ordering process for the low-temperature phase. Annealing experiments for prolonged times at 90 °C lead to further development of this phase structure, which always melts at around 100 °C in combination with minor transformation of the crystalline phases.

Furthermore, there is a broad exothermic process which occurs at around 145 °C after the low-temperature endothermic peak. The broad shape of this exothermic process indicates that this peak may include more than one thermal process (see below). A large endothermic peak can then be seen at around 170 °C. The heat of transition of this endothermic peak is 26.1 kJ/mol. If one carefully examines the DSC heating curve at 2.5 °C/min, this endothermic peak can also be observed, but with a much smaller heat of transition. At heating rates in excess of 2.5 °C/min, this endothermic peak cannot be seen. Since this temperature is more than 100 °C above the glass transition temperature, molecular motion should not be a determining factor for this phase transformation. Thus, this phase formation should be considered as an energy barrier controlled process, which is typically found in a crystallization process. Further heating leads to the high temperature endothermic onset at 193 °C which appears at every heating rate between 1 and 40 °C/min. Again, both the transition temperature and the heat of transition are heating rate independent. It should be pointed out that these DSC results are completely reproducible over multiple heating and cooling cycles.

These phase transitions which occur at a heating rate of 1 °C/min between 100 and 190 °C apparently do not take place during cooling at the same rate. This may be an indication that the high-temperature phase formed at 193 °C is only a low-ordered liquid crystalline phase and that this phase may only provide seeds but not have enough time to induce additional phase formations during cooling. After this phase is cooled slowly toward the glass transition temperature, a new low-temperature phase forms at 90 °C. Although it melts at an onset temperature around 100 °C during heating, development of other phases may overlap during or shortly after this melting process. However, DSC

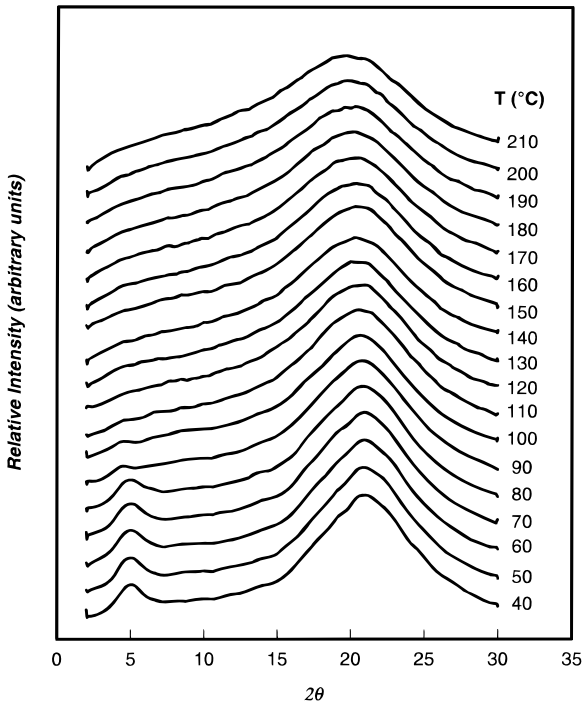

Figure 3. Set of PEBFP(n = 11) WAXD powder patterns during cooling at different temperatures (cooling rate of 1 °C/min).

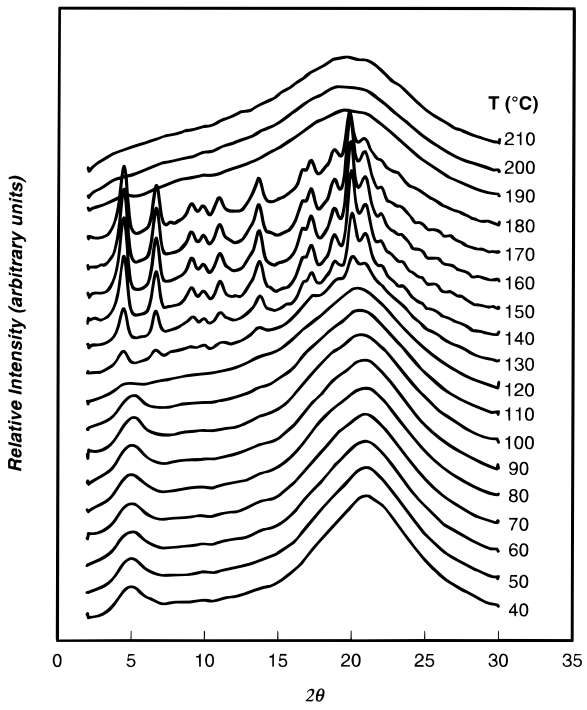

Figure 4. Set of PEBFP(n = 11) WAXD powder patterns during heating at different temperatures (heating rate of 1 °C/min).

experiments alone do not provide detailed structural identification of the phases and their phase relationships.

Phase Structural Changes. Figures 3 and 4 show two sets of WAXD powder patterns for the PEFBP(n = 11) sample at different temperatures during both cooling and heating at 1 °C/min. These data can be compared with the DSC heating and cooling diagrams performed at the same rate in order to recognize the phase structural changes which correspond to the thermal transitions. In Figure 3, WAXD cooling patterns from 210 °C do not provide any sharp Bragg reflections over the whole 2θ range from 1.5 to 30° when the temperature passes through the high-temperature exothermic peak (193 °C) in DSC. A sudden shift of the average d-spacing of a diffuse scattering halo around $2\theta = 20°$ can be observed. Note that the diffuse halo is a characteristic of the average distance between lateral chains. This phenomenon has been commonly seen in the case of the transitions from the isotropic melt (I) to a nematic (N) or a low-ordered smectic A or C (S_A or S_C) liquid crystalline state as in the cases of polymer synthesized from the coupling of 1-(4-hydroxyphenyl)-2-(2-methyl-4-hydroxyphenyl)ethane and odd-numbered α,ω-dibromoalkanes[19] and *N*-[4-(chloroformyl)phenyl]-4-(chloroformyl)phthalimide and different diols containing 4−12 methylene units (PEIM).[20] Therefore, the structural change which corresponds to the exothermic onset occurring at 193 °C in the DSC experiments (Figure 1) should be characterized as an I → N phase transition. Continuously decreasing the temperature does not introduce any sharp Bragg reflections until the temperature reaches 90 °C. At that temperature, a low-angle reflection at around $2\theta = 5°$ can be found, which corresponds to the low-temperature DSC exothermic peak (Figure 1). The correlation length of this low-angle reflection is 4 nm, which is smaller than traditional correlation lengths of a layer structure in a low-ordered polymer S_A or S_C phase. In the high-angle region, the width of half-height for the scattering halo decreases at 90 °C, indicating an increase in the correlation length of the lateral chain packing order. Although this low-angle reflection clearly indicates the formation of a new low-temperature phase, it is not certain at this moment whether this reflection represents a layer structure in this phase.

In heating, as shown in Figure 4, the low-temperature phase is retained until 110 °C. This phase then melts and the WAXD patterns return to the Bragg-featureless scattering (the N phase; see below). At 130 °C, new reflections start to appear in both the low- and high-angle regions with relatively weak intensities, indicating the formation of a new crystalline phase. At 140 °C, the WAXD Bragg reflection intensities suddenly increase and several new reflections appear such as at $2\theta = 16.6°$ and relatively weak reflections at $2\theta > 22°$. These observations indicate that this phase formed at 130 °C may only exist in a 10 °C temperature interval. Above that temperature, another new phase forms, which has somewhat different reflections and stronger reflection intensities from those of the previous phase at 130 °C. This new phase disappears at around 180 °C, and the WAXD patterns again show the Bragg-featureless scattering. At an even higher temperature of about 195 °C, a sudden shift of the d-spacing of the scattering maximum can be seen, indicating the transition to isotropization from the N phase.

In order to identify these three phases observed during cooling and heating experiments, isothermal WAXD experiments were also conducted. As shown in Figure 5, the three isothermal WAXD powder patterns after prolonged annealings represent three different ordered structures, confirming the phase structure changes based on WAXD cooling and heating experiments. Although the changes in phase structure during the transitions can be found in these WAXD powder experiments, they do not provide the structural symmetry and unit cell lattices due to the lack of dimensionality of these reflections. WAXD fiber patterns and

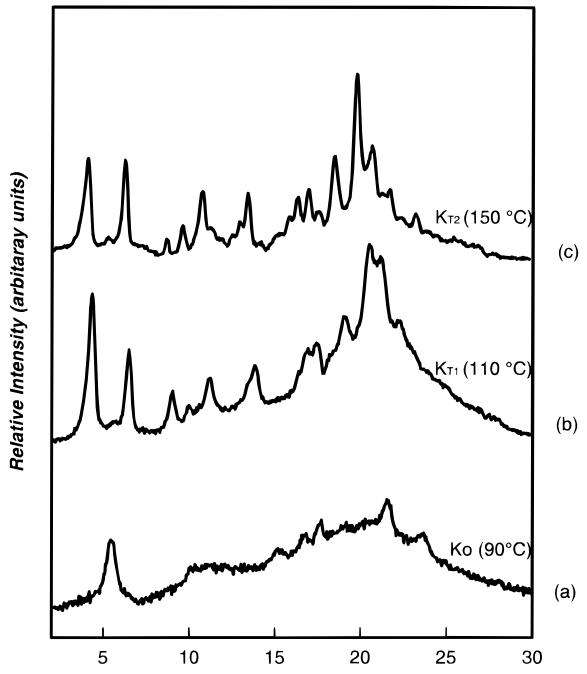

Figure 5. Three isothermal WAXD powder patterns of PEBFP(n = 11) at (a) 90 °C, (b) 110 °C, and (c) 150 °C, which are indications of three different ordered forms.

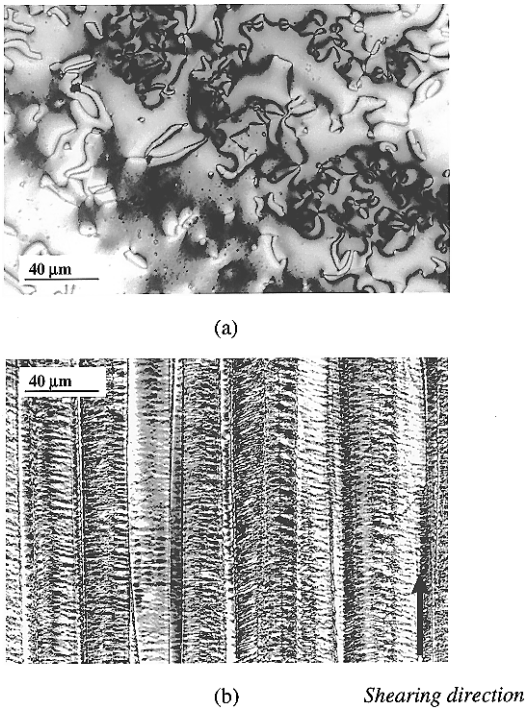

Figure 6. PLM micrograph of PEBFP(n = 11) for the high temperature nematic phase at 185 °C showing (a) unsheared monodomain schlieren texture and (b) sheared banded texture in film samples.

ED results are therefore necessary in order to classify these different states.

Phase Structural Identifications. The phase formed at 193 °C during cooling has been identified as an N phase using WAXD powder results. It can be further confirmed by using PLM morphological observations as shown in Figure 6. For a monodomain film sample at 185 °C, liquid crystalline defects are obvious, while for the sheared sample at that temperature, a banded texture is evidently perpendicular to the shear direction. Both morphologies reveal the existence of an

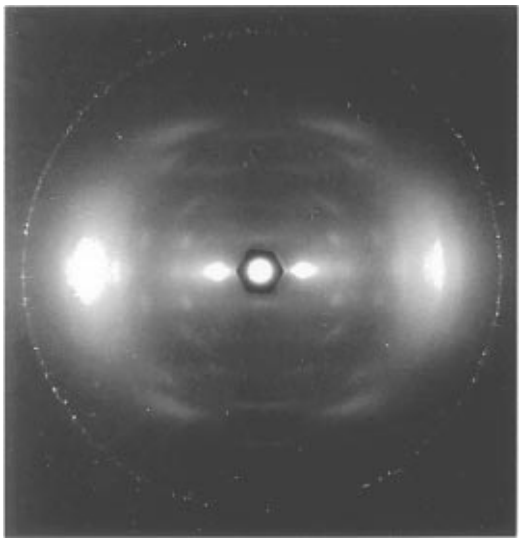

Figure 7. WAXD fiber pattern of a sample spun from the N phase and annealed at 90 °C.

N phase. In particular, the N phase morphology in Figure 6a is close to the morphology observed in cyanobiphenyl liquid crystals.[21] However, the heat of transition of the I ↔ N for polyacrylate(n = 11) containing cyanobiphenyl liquid crystals is 2.6 kJ/mol, while that of PEFBP(n = 11) is 2.4 kJ/mol. Note that in PEFBP(n = 11), the side groups only occupy 60% of the mass of the polymer. If this N phase is attributed solely to the cyanobiphenyl side group contribution, the heat of transition is thus calculated to be 1.6 kJ/mol, which is much lower than that of the polyacrylate(n = 11) analog. Furthermore, side-chain liquid crystalline polymers usually do not exhibit banded textures after mechanical shearing. These experimental facts indicate that the high-temperature N phase may be attributed to a combination of the cyanobiphenyl side chains and the main chain backbones of the polymer. When the monodomain sample is cooled to room temperature quickly, the liquid crystalline morphology is retained, and only a change can be found in the birefringence. However, if the sample is annealed at 90 °C for a prolonged time, a granular texture gradually develops and overrides the monodomain texture. This granular texture can be melted at 130 °C during heating to recover the monodomain texture. On the other hand, if we start with a polydomain sample which exhibits a granular texture at high temperature, a decrease of the granular size can be observed when the sample is annealed at 90 °C. Again, the original granular size can be recovered after the sample is heated up to 130 °C (melting of the low-temperature phase).

When fibers were annealed at a temperature of 90 °C, WAXD fiber patterns exhibit reflections not only on the equator and meridian but also in quadrant (Figure 7). Using the reciprocal lattice method, an orthorhombic unit cell can be deduced with dimensions of a = 1.61 nm, b = 1.04 nm, c = 2.10 nm, and $\alpha = \beta = \gamma = 90°$. The calculated crystallographic density is 1.236 g/cm^3, assuming it is two-chain orthorhombic. Due to the difficulty of obtaining ED from single crystals in this phase, the exact space group of this structure is not certain. Twenty-one experimentally observed reflections and their calculated 2θ, d-spacings, and intensities of reflections are available in Table 1 (in Supporting Information). Note that a hexagonal packing possesses a ratio between the a and b dimensions of a/b = 1.73. In this case, a/b = 1.55. We speculate that this phase

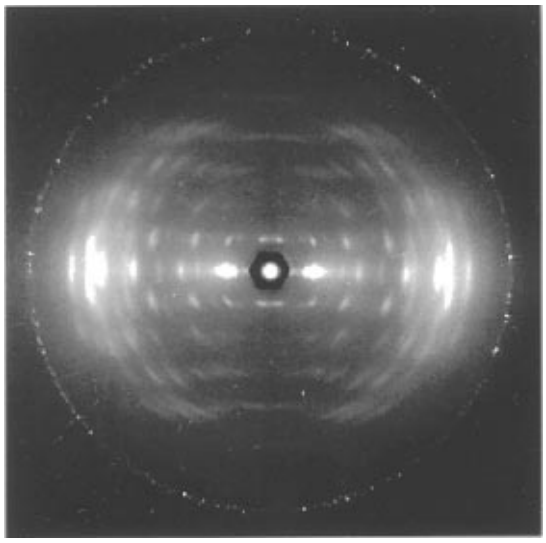

Figure 8. WAXD fiber pattern of a sample spun from the N phase and annealed at 115 °C.

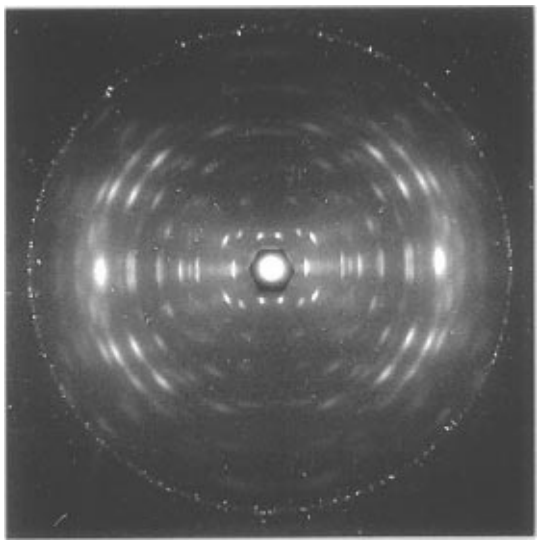

Figure 9. WAXD fiber pattern of a sample spun from the N phase and annealed at 150 °C.

may belong to a highly ordered smectic crystal or relatively poor crystal phase (the K_O phase).[22,23] This crystal phase corresponds to the WAXD powder patterns at 90 °C in Figure 5a. A careful analysis shows that these reflections in Figure 7 are more diffuse and weaker in comparison with typical WAXD fiber patterns of this polymer (see below). Their calculated correlation lengths are in a range from 4 to 5 nm. In particular, there is a pair of diffuse but strong equatorial reflections at around 1.70 nm ($2\theta = 5°$) on the equator, which corresponds to the broad reflection in WAXD powder patterns in the low-angle region (Figures 3 and 4). In fact, this pair of reflections possesses the strongest intensity among all of the reflections. One may speculate that this low-angle reflection represents a contribution from main-chain backbones aligned along the fiber direction. Between the main-chain backbones, the side chains reside, which lead to the difference in electron density and, therefore, form the periodicity of 1.70 nm perpendicular to the fiber direction. The cause of this pair of broad reflections on the equator is thus due to an intermolecular packing of the main chain backbones. Along the equator, another pair of diffuse scattering spots can also be observed at around 0.45 nm ($2\theta = 20°$), which represents the average *d*-spacing of the lateral packing between molecules.

When the annealing temperature is increased to 115 °C, the WAXD fiber pattern of PEFBP($n = 11$) changes drastically as shown in Figure 8. Sharp reflection spots can be seen, which correspond well with the powder pattern shown in Figure 5b. Its crystal lattice is determined to be triclinic with dimensions of $a = 1.93$ nm, $b = 1.73$ nm, $c = 2.08$ nm, $\alpha = 90°$, $\beta = 80°$, and $\gamma = 93°$. The crystallographic density is 1.266 g/cm^3, and four chains are included in one unit cell (the K_{T1} phase). Fifty-eight observed reflections and their calculated 2θ, *d*-spacings, and intensities are given in Table 2 (in Supporting Information). The temperature region over which this structure is stable is narrow (about 10 °C). Again, a reflection of 1.56 nm on the equatorial is attributed to the intermolecular packing of the main chain backbones. A pair of diffuse scattering halos at $2\theta = 20°$ are weak and illustrate the lateral molecular packing.

After further annealing at even higher temperatures of around 150 °C, another crystalline phase is observed (Figures 2 and 4). Figure 9 shows a WAXD fiber pattern of this crystalline phase. The reflection spots correspond well to the powder pattern in Figure 5c. A triclinic unit cell can be obtained with dimensions of $a = 1.90$ nm, $b = 1.74$ nm, $c = 2.04$ nm, $\alpha = 90°$, $\beta = 83°$, and $\gamma = 94°$. The calculated crystallographic density is 1.294 g/cm^3, and there are four chains in this triclinic lattice (K_{T2} phase). Seventy-three experimentally observed and calculated reflections as well as their intensities are listed in Table 3 (in Supporting Information). In this structure determination, the pair of low-angle reflections representing the intermolecular packing in both the K_O and K_{T1} phases are not observed. The diffuse scattering pair at $2\theta = 20°$ are almost undetectable, indicating a high crystallinity in this sample. It is interesting that this crystalline phase only differs from the K_{T1} phase in a rotation of the *b*-axis by 3°. The γ angle changes from 93° in the K_{T2} phase to 94° in the K_{T2} phase.

These two triclinic unit cell assignments are also supported by ED experiments in TEM as shown in Figure 10 for the K_{T1} phase and Figure 11 for the K_{T2} phase. Figure 10a shows the lamellar crystalline morphology of the K_{T1} phase grown at 110 °C, and its ED pattern of the [101] zone is shown in Figure 10b. This indicates that the chain axis is not perpendicular to the substrate due to the triclinic unit cell but is tilted by an angle of 7° with respect to the *a*-axis, since $\alpha = 90°$. Figure 10c is an ED pattern after the sample in Figure 10a is tilted by 38° to obtain the [001] zone diffraction. In Figure 11a, it is clear that single lamellar crystals can grow from the N phase at 150 °C. Figure 11b shows the ED pattern of the single crystals in Figure 11a. Since the unit cell is, again, triclinic, the direction of chain molecules is tilted 40° from the substrate normal and leads to a [101] zone diffraction. This figure provides an angle of 94° between the *a*- and *b*-axes. However, a tilt of 40° with respect to the *b*-axis in the ED experiments results in a [00l] zone diffraction as shown in Figure 11c. Detailed reflection assignments are also included in these figures.

We were puzzled as to whether these two crystal structures, the K_{T1} and K_{T2}, are truly representative of two different phases or if they actually belong to the same structure with a slight unit cell size change due to, for example, anisotropic thermal expansion. Two

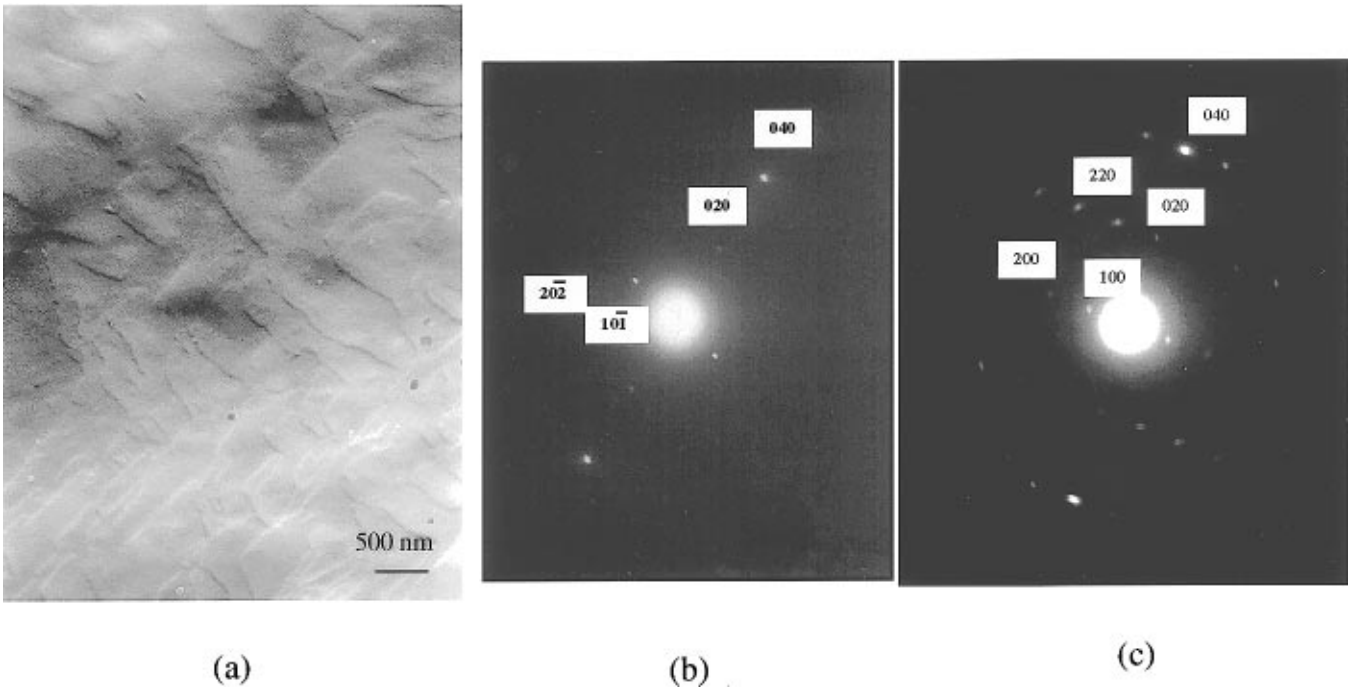

Figure 10. (a) PEFBP(n = 11) TEM and ED results for a (a) single lamellar crystal grown from the nematic phase at 110 °C and (b) the ED pattern along [101]zone and (c) the tilted ED pattern along [00l] zone.

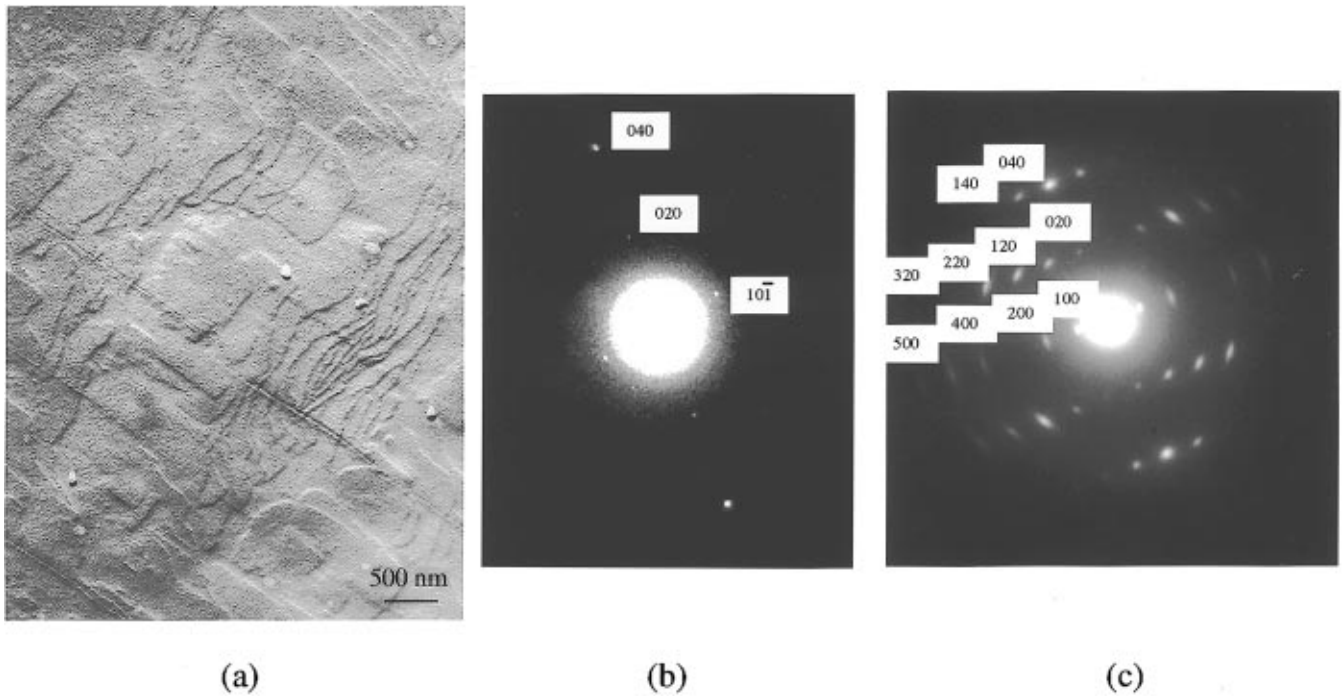

Figure 11. (a) PEFBP(n = 11) TEM and ED results for a (a) single lamellar crystal grown from thenematic phase at 150 °C and (b) the ED pattern along [101]zone, and (c) the tilted ED pattern along [00l] zone.

issues are important here. The first issue is how accurate our WAXD analyses are to unmistakably identify these two structures. The answer for the existence of these two structures is positive with a quite high degree of confidence based on the current condition of our WAXD facility. Note that the two WAXD fiber patterns in Figures 8 and 9 are quite different in terms of diffraction spot positions and intensities. For example, there are six reflections with strong or medium intensities in the K_{T1} fiber pattern which do not exist in the K_{T2} fiber pattern. On the other hand, there are 15 reflections with strong or medium intensities in the K_{T2} fiber pattern which cannot be found in the K_{T1} fiber pattern. Furthermore, the ED experiments also indicate the existence of the two structures.

The second issue deals with whether we have other independent experimental evidence to support the theory that there are two different phases. We have carried out a study of the phase transformation kinetics in a temperature region between 100 and 150 °C. If these two structures actually belong to one phase, the phase transformation kinetics should be represented as one growth rate branch. However, these two structures experimentally show distinguishable transformation kinetics with two completely independent growth branches. The growth rate of the K_{T1} phase between

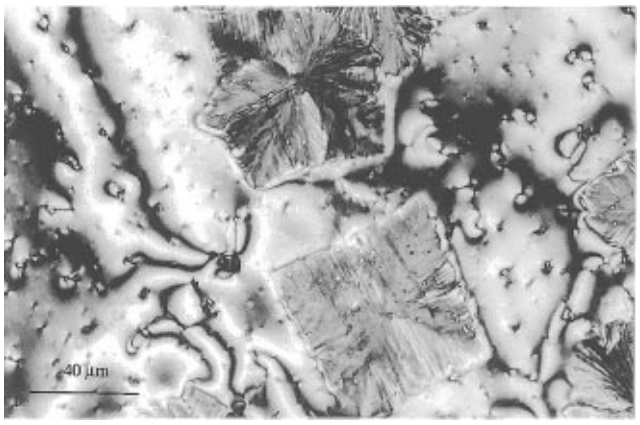

Figure 12. PLM micrograph of a PEFBP(n = 11) single lamellar crystal grown from thenematic phase at 150 °C.

100 and 110 °C is about several times to 1 order of magnitude slower than that of the K_{T2} phase between 120 and 140 °C. A sharp rate minimum exists at 110 °C. Our preliminary results from solid state carbon-13 nuclear magnetic resonance also indicate that the electron environments of the carbonyl, methylene, and phenylene carbon nuclei (chemical shifts) as well as mobility of the rigid components in cross-polarization spectra with magic angle spinning in the K_{T1} phase are substantially different from those of the K_{T2} phase. All of these results will be extensively discussed in future publications.

Although the majority of the crystalline morphology of the crystalline phase is composed of spherulites and axialites, it is also possible to grow sizable single lamellar crystals which can even be observed under PLM as shown in Figure 12. Not only is this dependent upon the crystallization conditions, but it °is also largely associated with the sample geometry and the substrate surfaces. A more or less rectangular shape can be observed. Careful measurement indicates that one of the angles of this single lamellar crystal is 80° and its corresponding supplementary angle is 100°. Note that in Figure 11b, the angle between the (020) and (10$\bar{1}$) is also 80°. This indicates that the single lamellar crystals observed in PLM as shown in Figure 12 also possess the [101] zone. The thickness of these single lamellar crystals is roughly 20−30 nm. This is also supported by the calculated correlation length of the (001) plane, which is approximately 25 nm. These values roughly correspond to the length of an extended backbone chain (a product of the degree of polymerization and repeating unit length, and the chain is 40° tilted from the subtract normal). We speculate that they are extended chain crystals. However, further experiments are necessary in order to obtain definitive conclusions.

Should these crystals be classified as sanidic liquid crystals? The definition of a sanidic or "boardlike" liquid crystals (Σ phase) shows four possible structures: Σ_{Ob}, $\Sigma_{Ou\perp}$, $\Sigma_{Ou\parallel}$, and Σ_{d}.[1,24] They represent positional orders which exist along both the chain and perpendicular to the chain directions, only along the direction perpendicular to the chain, only along the chain direction, and along neither of the directions, respectively. The molecules have a boardlike shape and associate into a layered structure. Dimensions of the *a*- and *b*-axes in a sanidic unit cell is thus very anisotropic. In our case, the molecular shape is not boardlike since two side chains are not on the same geometric plane. The two phenylene groups in the diols are twisted almost 90° away from each other due to the steric hindrance of the side chains at the 2- and 2′-positions of the phenylenes. The *a* and *b* dimensions of all three unit cells (the K_O, K_{T1}, and K_{T2} phases) are not substantially anisotropic. More importantly, in at least the K_{T1} and K_{T2} phases, (*hkl*) reflections are clearly shown, revealing that three-dimensional crystal structures do exist which can be resolved by classical crystallographic analyses. This implies that they are truly crystal solids rather than liquid crystalline states.

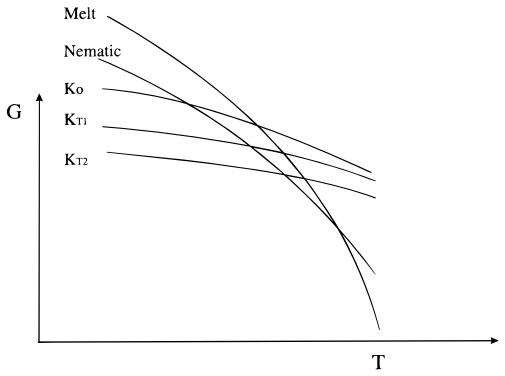

Figure 13. Thermodynamic relationships between the Gibbs free energy and temperature for the phases and phase transitions in PEFBP(n = 11).

Transition Thermodynamics and Structural Formation Mechanisms. In order to explain the complicated phase behavior which was observed in PEBFP(n = 11), it is important to correctly understand phase transition thermodynamics. Figure 13 systematically illustrates relationships between the Gibbs free energy and temperature for each of the phases and phase transitions between them. Note that the first derivative of the Gibbs free energy with respect to temperature is $-S$ (entropy) and the second derivative of this free energy with temperature is $-C_p/T$ (a ratio between heat capacity and temperature). These five phases are as follows: the I (isotropic) melt, the N phase formed by a combination of cyanobiphenyl side chain and backbones, the K_O phase, the K_{T1} phase, and finally the K_{T2} phase. The samples undergo the I → N transition during cooling since this is a near-equilibrium transition. However, the samples can bypass both the crystalline K_{T1} and K_{T2} phases and even the K_O phase at fast cooling rates. Only at a cooling rate of 10 °C/min or slower can the K_O phase form. This is due to the fact that, for the K_{T1} and K_{T2} phases, a nucleation process is necessary which requires undercooling to overcome the nucleation barrier for the development of these phases. The K_O phase forms close to the glass transition temperature of the polymer, and hampered molecular mobility may become the major factor which impedes the phase transformation. A similar observation has also been reported in the case of PEIM(n = 7) where the S_A phase transition temperature from the isotropic melt is only 11 °C higher than its glass transition temperature, and the transition kinetics are hampered mainly due to molecular motion.[25] When the samples are heated, the K_O phase melts first to enter the N phase, and shortly thereafter they further transfer to the K_{T1} phase. Next, the K_{T1} phase transfers to the K_{T2} phase. Finally, the K_{T2} phase melts to enter the N phase again, and this phase transfers to the isotropic melt at an even higher temperature.

It is important to notice that the K_O phase in this G *vs* T diagram (Figure 13) is monotropic with respect to both the K_{T1} and K_{T2} phases and that the K_{T1} is also

monotropic with respect to the K_{T2} phase. Therefore, the K_O and K_{T1} phases are thermodynamically metastable in the whole temperature region, and they are monotropic. Experimentally, the monotropic phase can be observed only if the stable phase is bypassed due to the necessity of undercooling required to overcome the free energy barrier during the transition. The K_O undergoes a melting process to return to the N phase before the K_{T1} phase is formed from this N phase, as observed in WAXD powder patterns (Figures 3 and 4). However, it is difficult to determine the transition behavior between the K_{T1} and K_{T2} phases due to the very narrow temperature region in which K_{T1} is kinetically stable. Further experiments are needed to explore this issue.

The remaining issue is to determine what role the side-chain methylene units play in these phase behaviors. Since both the glass transition and the crystal melting temperatures of the C_{11} are much lower than room temperature, it has been speculated in the past that the rigid polyester backbones reside in a medium of liquid alkyl chains. However, in this case, there is a cyanobiphenyl group on the end of each of the C_{11} side chains. It is known that cyanobiphenyl small molecules show liquid crystalline behavior with two types of packing (parallel and antiparallel). At high temperatures, it seems that the cyanobiphenyl side chains combine with the backbone chains to form the N phase which melts at 193 °C. Do cyanobiphenyl groups take part in the crystalline order in the K_{T1} and K_{T2} phases? If they do, what effect does that have on the methylene units? From our experimental structure analyses, it is evident that both the K_{T1} and K_{T2} phases possess high crystallinities of around 0.64 and 0.77 for bulk samples and 0.70 and 0.85 for fiber samples, respectively. Note that the main chain backbones only occupy 40% of the overall weight of the polymer. Even if both the cyanobiphenyl groups and the backbone chains are fully crystallized, they only count for 76% of the overall weight of the polymer, which is lower than 0.85 crystallinity in the fiber samples. Specifically, few traces of nematic and amorphous scattering at around $2\theta = 20°$ can be found in the WAXD fiber pattern of the K_{T2} phase. It is speculated, therefore, that the methylene units may also be included in the crystalline lattice. However, solid-state carbon-13 nuclear magnetic resonance experiments and detailed atomic structure simulation must be conducted in order to understand the molecular mobility of different carbon nuclei and the molecular and supramolecular packing in the different crystal unit cells. These works are currently under investigation.

Conclusion

We have reported complicated phase behavior in a rigid-rodlike polyester which consists of C_{11} methylene units with cyanobiphenyl end groups. Five different phase structures which exist in this polymer have been identified utilizing combined techniques of WAXD, ED, and morphological observations under PLM and TEM. In decreasing temperature sequence, they are as follows: the I (the isotropic melt), the N (the nematic liquid crystal phase), the K_{T2} (the high temperature triclinic crystalline phase), the K_{T1} (the low temperature triclinic crystalline phase), and the K_O (the highly ordered smectic crystal or relatively poor crystal having an orthorhombic lattice) phases. The phase transitions can be understood using thermodynamics (the plot of Gibbs free energy *vs* temperature) and kinetic effects (undercooling dependence due to crystal nucleation and slow molecular motion due to temperatures close to that of the glass transition). Among them, the K_O and K_{T1} phases are monotropic with respect to the K_{T2} phase. It is speculated that the cyanobiphenyl side chains may play an important role in the formation and stabilization of these different phases.

Acknowledgment. This work was supported by the National Science Foundation (DMR-9157738 and 9617030) and the Science and Technology Center for Advanced Liquid Crystal Optical Materials (ALCOM) at Kent State University, Case Western Reserve University, and the University of Akron.

Supporting Information Available: Three tables containing detailed information about observed and calculated data of 2θ, d-spacing, and relative intensities of WAXD reflections for three crystal structures (5 pages). See any current masthead page for ordering information.

References and Notes

(1) Herrmann-Schonherr, O.; Wendorff, J. H.; Ringsdorf, H.; Tschirner, P. *Makromol. Chem. Rapid Commun.* **1986**, *7*, 791.
(2) Ballauff, M.; Schmidt, G. F. *Makromol. Chem. Rapid Commun.* **1987**, *8*, 93.
(3) Berger, K.; Ballauff, M. *Mol. Cryst. Liq. Cryst.* **1987**, *147*, 163.
(4) Cervinka, L.; Ballauff, M. *Colloid Polym. Sci.* **1992**, *270*, 859.
(5) Adam, A.; Spiess, W. *Macromol. Chem. Rapid Commun.* **1990**, *11*, 249.
(6) Frech, C. B.; Adam, A.; Falk, U.; Boeffel, C.; Spiess, W. *New Polym. Mater.* **1990**, *2*, 267.
(7) Clauss, J.; Schmidt-Rohr, K.; Adam, A.; Boeffel, C.; Spiess, W. *Macromolecules* **1992**, *25*, 5208.
(8) Kricheldorf, H. R.; Domschke, A. *Macromol. Chem. Phys.* **1993**, *195*, 943, 957.
(9) Kricheldorf, H. R.; Domschke, A. *Polymer* **1994**, *35*, 198.
(10) Watanabe, J.; Ono, H.; Uematsu, I.; Abe, A. *Macromolecules* **1985**, *18*, 2141.
(11) Kricheldorf, H. R.; Domschke, A. *Macromolecules* **1996**, *29*, 1337.
(12) Kim, H.; Park, S.-B.; Jung, J. C.; Zin, W.-C. *Polymer* **1996**, *37*, 2845.
(13) Watanabe, J.; Sekine, N.; Nematsu, T.; Sone, M.; Kricheldorf, H. R. *Macromolecules* **1996**, *29*, 4816.
(14) Wang, S.-Y. Ph.D. dissertation, Department of Polymer Science, The University of Akron, Akron, Ohio 44325-3909, 1995.
(15) Beguin, A.; Billard, J.; Bonamy, F.; Buisine, J. M.; Cuvelier, P.; Dubois, J. C.; Le Barny, P.; *Mol. Cryst. Liq. Cryst.* **1984**, *115*, 122.
(16) Shibaev, V. P.; Kostromin, S. G.; Plate, N. A. *Eur. Polym. J.* **1982**, *18*, 651.
(17) Kawakami, Y.; Takahashi, K.; Hibino, H. *Macromolecules* **1991**, *24*, 4531.
(18) Eashoo, M.; Wu, Z.; Zhang, A.; Shen, D.; Tse, C.; Harris, F. W.; Cheng, S. Z. D.; Gardner, K. H.; Hsiao, B. S. *Macromol. Chem. Phys.* **1994**, *195*, 2207.
(19) Yandrisits, M. A.; Cheng, S. Z. D.; Zhang, A.-Q.; Cheng, J.; Wunderlich, B.; Percec, V. *Macromolecules* **1992**, *25*, 2112.
(20) Pardey, P.; Shen, D.; Gabori, P. A.; Harris, F. W.; Cheng, S. Z. D.; Adduci, J.; Facinelli J. V.; Lenz, R. W. *Macromolecules*, **1993**, *26*, 3687.
(21) Patel, J. S.; Yokoyama, H. *Nature* **1993**, *362*, 525.
(22) Gray, G. W.; Goodby, J. W. G. *Smectic Liquid Crystals*, Leonard Hill: London, 1984.
(23) Pershan, P. S. *Structure of Liquid Crystal Phases*; World Scientific: Singapore, 1988.
(24) Ebert, M.; Herrmann,-Schenherr, O.; Wendorf, J. H.; Ringsdorf, H.; Tschirner, P. *Liq. Cryst.* **1990**, *7*, 63.
(25) Pardey, R.; Wu, S. W.; Chen, J.; Harris, F. W.; Cheng, S. Z. D.; Keller, A.; Aducci, J.; Facinelli, J. V.; Lenz, R. W. *Macromolecules* **1994**, *27*, 5794.

MA970611K